# Scaling of H-mode energy confinement with $I_p$ and $B_T$ in the MAST spherical tokamak

M. Valovič, R. Akers, G. Cunningham, L. Garzotti, B. Lloyd, D. Muir, A. Patel,
D Taylor, M. Turnyanskiy, M. Walsh and the MAST team

EURATOM/UKAEA Fusion Association, Culham Science Centre, Abingdon, Oxon OX14 3DB, UK

e-mail contact of main author: martin.valovic@ukaea.org.uk

**Abstract**

The dependencies of energy confinement on plasma current and toroidal magnetic field have been investigated in the MAST spherical tokamak in H-mode plasmas. Multivariate fits show that the dependence of energy confinement time on plasma current $I_p$ is weaker than linear while the dependence on toroidal magnetic field $B_T$ is stronger than linear, in contrast to conventional energy confinement scalings. These $I_p$ and $B_T$ dependencies have also been confirmed by single parameter scans. Transport analysis indicates that the strong $B_T$ scaling of energy confinement could possibly be explained by weaker $q$ and stronger $\nu_*$ dependence of heat diffusivity in comparison with conventional tokamaks.

**PACS Numbers**: 52.55.Fa, 52.25.Fi

## 1. Introduction

Energy confinement time plays a central role in design of tokamak fusion reactors. Energy confinement scalings derived from the database of tokamaks with conventional aspect ratio, such as IPB98(y,2) [1], display strong (linear) dependence on plasma current. As a result plasma current is the main driver in design of conventional aspect ratio fusion reactors such as ITER and demonstration power plants [2, 3]. Confinement scaling derived from conventional tokamaks has been also used in design of fusion reactors based on low aspect ratio tokamaks. Future low aspect ratio tokamak reactors are foreseen as compact volume neutron sources that can be used, for example, to test components for fusion power plants. An example of such a device is a Component Test Facility based on the spherical tokamak (ST-CTF) [4]. The use of conventional aspect ratio scalings for devices like ST-CTF had some support from the earlier observations that the values of energy confinement time in low aspect ratio tokamaks MAST and NSTX broadly agree with those predicted by the IPB98(y,2) scaling [5, 6]. Nevertheless more detailed analysis shows that some parametric dependencies of energy confinement in

low aspect ratio tokamaks are different than predicted by IPB98(y,2) scaling. For example favourable collisionality dependence was found in MAST [5] and NSTX data [7], and strong (linear) dependence on toroidal magnetic field was reported in NSTX [8]. These differences might change the role of various plasma parameters in optimisation of fusion reactors based on low aspect ratio tokamaks.

This paper concentrates on the scaling of the energy confinement time with plasma current and toroidal magnetic using the H-mode data obtained from MAST tokamak.

## 2. Experimental conditions

The dataset used for this study expands significantly the parameter range in comparison with our most recent publication [5], in particular towards higher heating powers and higher plasma current. The data consist of ELMy and ELM-free H-mode plasmas with double null divertor configuration. The engineering parameters span the following intervals: plasma current $I_p = (0.60-1.17)MA$, geometric major radius $R_{geo} = (0.77-0.90)m$, minor radius $a = (0.54-0.62)m$, elongation $\kappa = 1.7-2.0$, triangularity $\delta = 0.4-0.5$, vacuum toroidal field at the geometric radius $B_T = (0.34-0.50)T$ and line averaged density $\overline{n}_e = (2.1-5.4)\times 10^{19} m^{-3}$. The working gas is deuterium. Plasmas are heated with neutral beams with injected power of $P_{NBI} = (1.2-3.5)MW$ with energy of $\leq 67\,keV$. The beams are injected in the direction of plasma current. Sawteeth are avoided by application of neutral beam heating during the current ramp-up. This is different from the majority of data in the conventional multi-machine database which is dominated by sawtoothing plasmas [1]. Data on energy confinement are extracted at times close to the flat top of energy content in order to minimise the uncertainty due to the time derivative of energy content. Only one data point per shot is taken and the dataset consists of $N = 97$ data points.

## 3. Multivariate scaling of total energy confinement

The dataset of H-mode plasmas described above has been firstly analysed by an ordinary least square regression fit (OLS) using the logarithms of the variables. The scaling is chosen in the form of $W_{mag} = C\, I_p^{\alpha I}\, B_T^{\alpha B} \overline{n}_e^{\alpha n} P_L^{\alpha P}$. Here, $W_{mag}$ is the energy content from equilibrium reconstruction (EFIT) and $P_L = P_{ohm} + P_{NBI} - d\,W_{mag}/dt$ is the power loss where $P_{ohm}$ is the ohmic power, $P_{NBI}$ is the injected beam power. Beam shine through and

unconfined orbit losses, calculated for representative shots by the TRANSP code [9], are a few percent [5] and are neglected in this part of the analysis. Radiated power ($<13\%$ of $P_L$) is not included in confinement scaling laws by a convention used in the international tokamak confinement database [1]. The reason to choose the total energy content as a regression variable instead of energy confinement time is to simplify the discussion of the role of collinearities and measurement errors. The scaling obtained by ordinary least square regression fit is:

$$W_{mag,OLS\ fit} = 0.252\, I_p^{0.59}\, B_T^{1.4} \bar{n}_e^{0.00} P_L^{0.27} \qquad \text{(RMSE=12.1\%)} \qquad (1)$$

where the units are MJ, MA, T, $10^{19} m^{-3}$ and MW respectively. The quality of the fit is shown in figure 1.

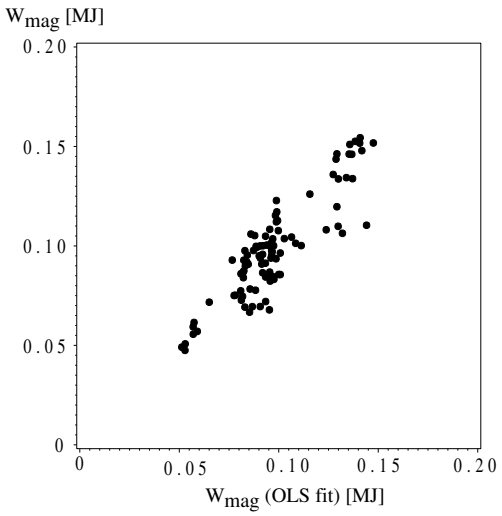


Figure 1. Regression analysis to total energy content (exponents are given in equation 1).

It is seen that the scaling shows much stronger dependence on toroidal magnetic field than the scalings derived from databases of conventional tokamaks while the scaling with plasma current is somewhat weaker. For example in IPB98(y,2) scaling the dependence of (thermal) energy content on toroidal magnetic field and plasma current is: $W_{th} \propto I_p^{0.93} B_T^{0.15}$ [1].

A common problem with multivariate fits is that datasets are not well conditioned to extract all exponents due to the correlations between variables. To assess the conditions in our database, a principal component analysis (PCA) on a set of independent variables ($I_P$, $B_T$, $\bar{n}_e$, $P_L$) was performed. It is well known that the size of the bias in the OLS fits caused by a

particular principal component (PC) is equal to the square of the error-to-variance ratio: $\sim\left(\lambda_e/\lambda_{pc}\right)^2$ [10, 11]. Here, $\lambda_{pc}$ is the standard deviation of a PC and $\lambda_e$ denotes the standard deviation of particular PC due to the errors in engineering parameters. In our case the errors in engineering variables are estimated as: $\delta I_P \approx 1\%$, $\delta B_T \approx 1.5\%$, $\delta \overline{n}_e \approx 7\%$, $\delta P_L \approx 10\%$. The result of the principal component analysis using a covariance matrix is shown in table 1. It is seen from the table that two parameters of our interest, plasma current and toroidal magnetic field, are mainly linked to the last two PCs as $PC3 \propto \ln(I_p^{0.8})$ and $PC4 \propto \ln(B_T^{0.9})$, as highlighted by bold in Table 1. These two PCs have $(\lambda_e/\lambda_{pc})^2$ = 9% or 12%, respectively. These errors, crudely speaking, translate to uncertainties of the same magnitude in the $\alpha_I$ and $\alpha_B$ exponents, respectively, in the OLS fit. Such database conditions are rather typical. For example in the latest multi-machine ITPA H-mode confinement database, with 3093 observations and 8 engineering parameters, the error-to-variance ratio $(\lambda_e/\lambda_{pc})^2$ is below 6% only for the first 3 principal components, for another 3 PCs it is in the range 11-17% and for rest it is above 100% [12].

Table 1. Principal components of the $N = 97$ dataset together with their standard deviations $\lambda_{pc}$, errors $\lambda_e$ and the square of error-to-variance ratios $(\lambda_e/\lambda_{pc})^2$.

| | $\ln(I)$ | $\ln(B)$ | $\ln(n)$ | $\ln(P)$ | $\lambda_{pc}$ | $\lambda_e$ | $(\lambda_e/\lambda_{pc})^2$ |
|---|---|---|---|---|---|---|---|
| PC1 | 0.379 | 0.015 | 0.480 | 0.790 | 0.33 | 0.086 | 0.068 |
| PC2 | 0.426 | 0.319 | 0.612 | -0.583 | 0.21 | 0.073 | 0.12 |
| PC3 | **0.769** | 0.163 | -0.617 | 0.003 | 0.14 | 0.044 | **0.094** |
| PC4 | -0.286 | **0.933** | -0.109 | 0.186 | 0.071 | 0.025 | **0.12** |

A second well known problem with OLS regression is that it can give biased results if independent variables have errors comparable with the error of the dependent variable. This is clearly our case where the error in energy content $\delta W_{mag} \approx 10\%$ is comparable with the errors in density and power loss as given above. This problem is usually dealt with by an application of principal component analysis and error-in-variable method (PCEIV) [10, 11]. In this technique all variables, including energy content, are put into a single set and the logarithms of all variables are weighted by an inverse of their relative errors. Then the exponents in the scaling are found from the coefficients corresponding to the principal component having the

smallest variation. The result of such a fitting procedure for the same dataset as used for scaling (1) is:

$$W_{mag,PCEIV} \propto I_p^{0.51} B_T^{1.6} \bar{n}_e^{-0.06} P_L^{0.39} \quad (2)$$

It is seen that in our case, the PCEIV method gives rather similar results to the OLS regression (1). The differences in exponents are in the range of uncertainties predicted by the principal component analysis (PCA) given above.

## 4. Single parameter $I_P$ and $B_T$ scaling

### *4.1 $I_P$ scan*

To encapsulate the $I_P$ dependence separately from the rest of the engineering parameters we have narrowed the dataset described in section 3 so that it represents essentially a single parameter scan along $I_P$ . The range of toroidal magnetic field is narrowed to $B_T = (0.44 - 0.49)T$ and the dataset is restricted only to plasmas heated by 2 beam lines, $P_{NBI} = (3.0 - 3.2)MW$ . The range of line-averaged plasma electron density has to be relatively wide, $\bar{n}_e = (2.8 - 4.5) \times 10^{19} m^{-3}$, in order to keep enough data points in the scan. In the first order approximation, the wider density range is justified by the fact that the multi-parameter scalings (1) and (2) indicate a weak density dependence of energy content. (The uncertainty due to density dependence will be completely removed in section 5 below using two point scans.) The result of this narrowing procedure is a dataset with $N_{Ip} = 11$ data points in which the plasma current changes by a factor of 1.95.

The result of this single parameter plasma current scan is shown in figure 2. The log-linear regression fit to the dataset gives the plasma current scaling as $W_{mag} \propto I_p^{0.6 \pm 0.3}$ which is in good agreement with the four parameter fits (1) and (2) given in the previous section. Here the error in the exponent is not a statistical error of OLS fit, but the min-max ranges based on two extreme cases. These extremes correspond to the minimum and maximum slopes that can be drawn through the data points as indicated by dotted lines in figure 2. The reason for this choice is that the statistical errors given by OLS procedure are typically small and do not reflect internal correlations in the dataset. This will be discussed in section 5 below. Figure 2 also shows that the possible error due to the finite range of toroidal magnetic field is smaller than the uncertainty in the exponent of the current dependence. This is evident from the small difference between the measured values of energy content (open symbols in figure 2) and

corrected values of energy content using the assumption that the dependence on magnetic field is $W_{mag} \propto B_T^{1.5}$ (full symbols in figure 2).

Similar analysis has been performed using the electron energy content $W_{e,kin}$ calculated from Thomson scattering profiles. Analysis shows that $W_{e,kin}$ depends on plasma current as $W_{e,kin} \propto I_p^{0.5\pm0.4}$ , i. e. similar to total energy content dependence (seen in figure 2). Again the error in the exponent is the min-max range based on extreme cases of the slopes. It is also seen that the ratio between total and electron energy contents is $W_{mag} \approx 2.7 \times W_{e,kin}$ and it is constant along the $I_p$ range. Writing the total energy content as $W_{mag} = W_{e,kin} + W_{i,kin} + W_{fast,i}$ $= W_{th} + W_{fast,i} \approx 2W_{e,kin} + W_{fast,i}$ , such a ratio is consistent with the thermal energy content of $W_{th} \approx 0.74 W_{mag}$ and fast ion content of $W_{fast,i} = 0.26 W_{mag}$ . This fraction of thermal to magnetic energy contents is in agreement with the value found by TRANSP analysis for two point scans in sections 5 and 6 below.

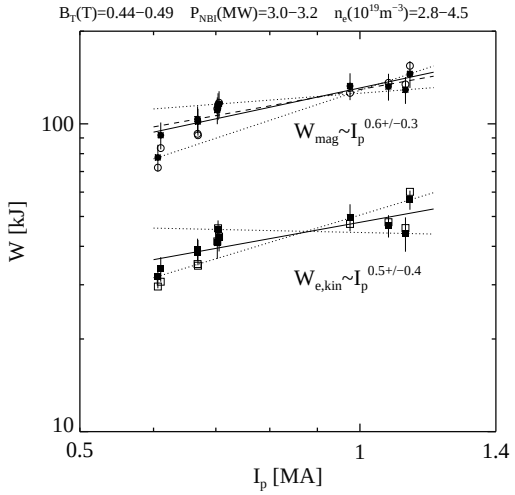


Figure 2. Dependence of total and electron energy contents on plasma current. Full symbols are data corrected for small differences in $B_T$ assuming $W_{mag} \propto W_{e,kin} \propto B_T^{1.5}$ , open symbols are uncorrected data. The full lines are the regression fits. Dotted lines represent the minimum and maximum of possible slopes. The dashed line is $2.7 \times W_{e,kin,fit}$ .

*4.2 $B_T$ scan*

Similar analysis as described above has been applied to the dependence of energy content on the vacuum toroidal magnetic field $B_T$ . For this purpose the range of plasma current is narrowed to $I_p = (0.60 - 0.71) MA$ . Again only plasmas heated with two beam lines are selected so that $P_{NBI} = (2.8 - 3.2) MW$ . The range of line-averaged plasma electron density is relatively wide, $\overline{n}_e = (2.6 - 4.5) \times 10^{19} m^{-3}$ to ensure enough data points in the scan. The

resulting dataset has $N_{BT} = 13$ data points and the toroidal magnetic field varies by a factor of 1.44.

Log-linear regression for total energy content gives $W_{mag} \propto B_T^{1.4\pm0.6}$ as shown in figure 3. Here again the error in exponent is the envelope of the possible slopes. It is seen that within this uncertainty, the single parameter $B_T$ scan is in agreement with the multivariable fits given by equations (1) and (2). The error due to the finite range of plasma current in the dataset is small as seen from the size of the corrections to the energy content if one assumes a plasma current dependence of the form $W_{mag} \propto I_P^{0.6}$.

Electron energy content scales with toroidal magnetic field as $W_{e,kin} \propto B_T^{1.8\pm0.7}$, with the error being again the min-max estimate of the slopes in the log-log diagram. The ratio between total energy content from magnetic equilibrium and electron energy content is similar to that found in the single parameter $I_P$ scan, $W_{mag} \approx 2.7 \times W_{e,kin}$.

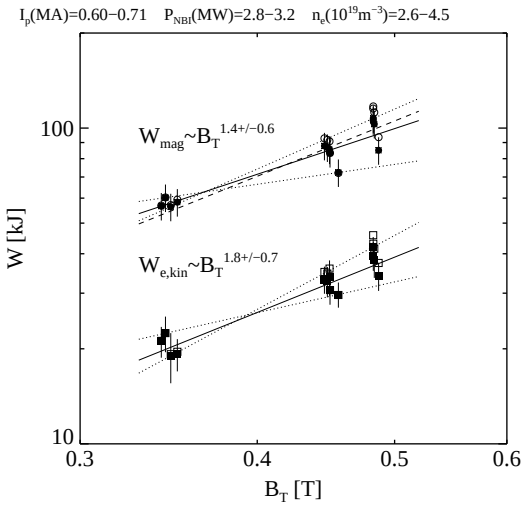


Figure 3. Dependence of total and electron energy contents on toroidal field. The full symbols are data corrected for small differences in $I_p$ assuming $W_{mag} \propto W_{e,kin} \propto I_P^{0.6}$, open symbols are uncorrected data.The full lines are the regression fits. The dashed line is $2.7 \times W_{e,kin\_fit}$.

## 5. Two point $I_P$ and $B_T$ scans

As mentioned in the previous section, even the narrowed dataset used for single parameter scans can be affected by correlations that could influence the scalings. Detailed inspection of the datasets in figures 2 and 3 reveals that the density range is not narrow enough to eliminate such a possibility. In particular, the dataset utilised for the single parameter $I_P$ scan, suffers from very low ELM frequency for plasmas with $I_P > 1MA$ and as a result these plasmas have

higher density than plasmas with lower values of $I_P$. Similar correlations exists in the dataset utilised for the single parameter $B_T$ scan: plasmas with higher $B_T$ tend to have higher densities than plasma with lower toroidal field. To eliminate this we have narrowed the datasets further just to 2-point scans. For each pair the density, power and either $B_T$ or $I_P$ were matched as close as possible and then a heat transport analysis was performed.

*5.1 $I_P$ scan*

The result of the two point $I_P$ scan is shown in figure 4. For both plasmas, $B_T = 0.45T$ and also the density profiles are matched very well. To obtain this, however, the range of $I_P$ has to be reduced to a factor of 1.6 compared to nearly a factor of 2 in the multipoint $I_P$ scan in section 4.1 above. The pair has been analysed using the TRANSP code. TRANSP is used to calculate the radial profile of total heat flux density, $q_T$. Here $q_T$ is the sum of electron and ion fluxes and includes both conductive and convective components. It has to be pointed out that to subtract the convective component would require detailed particle source analysis. Nevertheless it is found that for typical neutral densities at the plasma edge the contribution from the convective flux is small and is localised at the outer edge of the confinement region. The heat transport analysis shows that there is a slight mismatch in the total heat flux between the two plasmas (figure 4b). This is caused by different ohmic powers at different values of $I_P$. To extract the dependence on plasma current in this situation we assume that the energy content scales with the power loss as $\propto P_L^{1/3}$ in line with the scalings (1) and (2). Using this correction the comparison of electron energy contents gives

$$W_{e,kin} \propto I_p^{0.63} P_L^{1/3}. \qquad (3)$$

Note that the ratio of energy contents is given be the ratio of electron temperatures $T_e$ (fig. 4c) as the densities are well matched. Scaling (3) is in good agreement with the multivariate scaling in section 3 and the single parameter scan in section 4.1. The ion temperature $T_i$ in this scan is measured by a neutral particle analyser and within the error bars $T_e \approx T_i$ (fig. 4c). Effective ion charge $Z_{eff}$ is measured by visible bremstrahlung emission and $Z_{eff} \approx 1$ throughout the whole plasma cross section. This suggests that the thermal energy content $W_{th} \propto W_{e,kin}$.

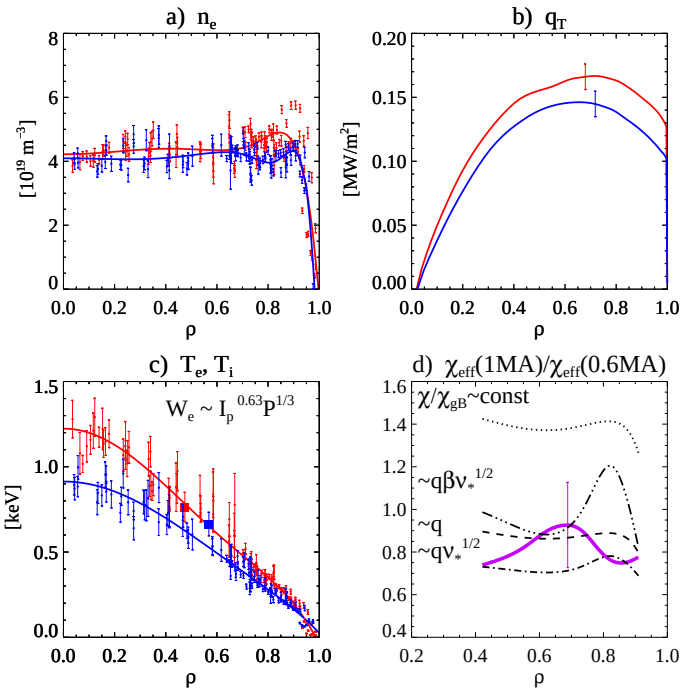


Figure 4. Transport analysis of $I_P$ scan. $I_P = 0.97MA$ (red symbols) and $I_P = 0.61MA$, (blue symbols). $B_T = 0.45T$, $\rho = \psi_N^{0.5}$, where $\psi_N$ is the normalised poloidal magnetic flux. (a): density profiles as measured by Thomson scattering (b): total heat flux $q_T$. (c): symbols with error bars are $T_e$, square symbols are $T_i$ from NPA. (d): pink line is the ratio of experimental diffusivities, black lines are the ratios expected from different models calculated from $n_e$ and $T_e$ profiles and with $q \sim B_T/I_p$.

*5.2 $B_T$ scan*

Fig. 5 shows similar analysis for the $B_T$ scan. For both plasmas, the current, electron density and heat flux density $q_T$ are the same within the error bars. The ratio of electron energy contents results in a scaling of

$$W_{e,kin} \propto B_T^{1.3}. \qquad (4)$$

Again the ratio of electron energy content is given by the ratio of electron temperatures (figure 5c). The scaling (4) is in line with the result of the multivariate analysis in section 3 and the single parameter scan in section 4.2.

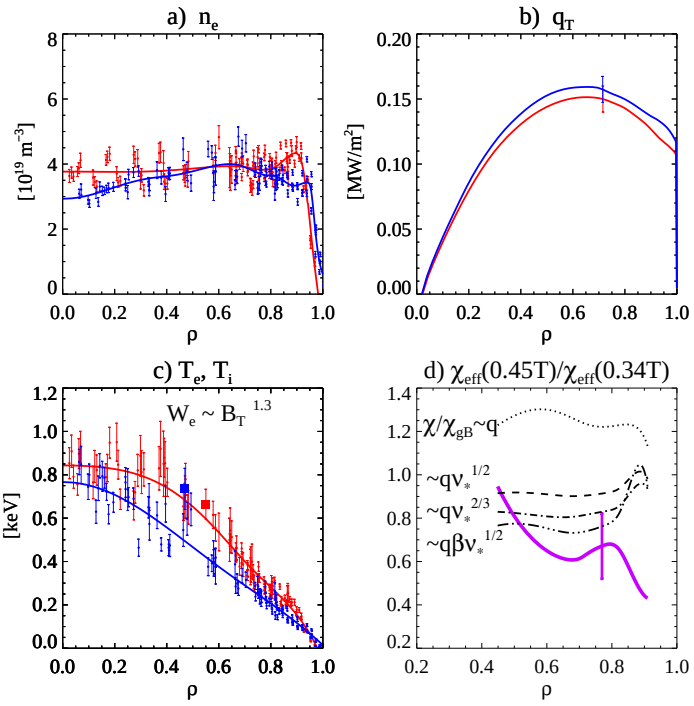


Figure 5. Transport analysis of $B_T$ scan. $B_T = 0.45T$ (red symbols) and $B_T = 0.34T$ (blue symbols). $I_p = 0.61MA$. Other notation as in fig. 4.

## 6. Interpretation of $I_P$ and $B_T$ scalings by dimensionless parameters

Within the framework of power law formulas the energy confinement can be expressed in terms of dimensionless plasma physics parameters as $\tau_E B_T \propto \rho_*^{x_\rho} q^{x_q} \beta^{x_\beta} \nu_*^{x_\nu}$. Here, $\rho_*$ is the normalised Larmor radius, $q$ is the engineering safety factor, $\beta$ is the toroidal beta and $\nu_*$ is the collisionality. Here, $\rho_*$, $\beta$ and $\nu_*$ are the conventional global dimensionless parameters in which the average plasma temperature $T$ is defined from the ratio of energy content and line average plasma density [1]. Here the collisionality is defined as $\nu_* \propto \bar{n}_e / T^2$, i. e. without the $q$ dependence to simplify the discussion. Formally the exponents in the dimensionless scaling law can be calculated from exponents in the scaling in engineering parameters. However, it is well known that dimensionless scalings are sensitive to small errors in the exponents in engineering parameters. Therefore if the dataset is not ideally conditioned then formal mapping of scalings from engineering parameters to dimensionless parameters could provide confusing results. This is clearly our case where the mapping of scaling (1) gives $\tau_E B_T \propto \rho_*^{-4.4} q^{-2.1} \beta^{-1.9} \nu_*^{-0.74}$, where the dependencies on $\rho_*$ and $\beta$ are unusually strong. This is a consequence of the fact that in the present dataset the dimensionless variables are correlated, in particularly the largest Pearson correlations are $corr(\rho_*, \beta) = 0.49$ and $corr(\beta, q) = -0.67$, so that the corresponding exponents are poorly determined simultaneously. To proceed further

we will assume in rest of this section that the energy confinement and heat transport is gyro-Bohm so that $\tau_E B_T \propto \rho_*^{-3} q^{x_q} \beta^{x_\beta} \nu_*^{x_\nu}$.

The main result of previous sections is that the dependence of energy confinement on toroidal magnetic field is much stronger than in the conventional scaling IPB98(y,2) and the dependence on plasma current is weaker than in IPB98(y,2). This seeming interplay, however, can not be interpreted only as a poorly resolved $q$ dependence in our database, that is typically the case for datasets with similar $q$. The separation of $I_P$ and $B_T$ dependencies is discussed later but the difference between MAST and conventional scaling is already apparent from the fact that the sum of the $I_P$ and $B_T$ exponents in MAST is 2 times larger than in the IPB98(y,2) scaling. More precisely, for MAST, equations (1), (2), (3) and (4) give $\alpha_I + \alpha_B = 1.93 \div 2.11$ while in IPB98(y,2) scaling this sum is $\alpha_I + \alpha_B = 1.07$. This difference can be interpreted from the following relationship between the exponents in dimensional and dimensionless scalings:

$$\alpha_B + \alpha_I = \left(2 - 2x_\beta\right) \Big/ \left(\frac{5}{2} - x_\beta + 2x_\nu\right) \tag{5}$$

Here, gyro-Bohm transport is assumed. It is seen from (5) that the sum $\alpha_I + \alpha_B$ is controlled mainly by the collisionality exponent $x_\nu$. For collisionality-independent scaling, $x_\nu = 0$ (similar to IPB98(y,2) ), the sum is $\alpha_B + \alpha_I = 0.8 \div 1.1$, where the range corresponds to $\beta$ scalings in the range of $x_\beta = -1 \div 0$. On the other hand for strong collisionality dependence with $x_\nu = -3/4$, the sum is $\alpha_B + \alpha_I = 2$, i.e. close to the MAST value, and does not depend on $x_\beta$. It is interesting to note that this strong collisionality dependence is also consistent with the zero or even slightly negative density exponent in equations (1) and (2). This can be seen from the transformation between dimensionless exponents and density scaling: $\alpha_n = \left(3/2 + 3x_\nu\right) \Big/ \left(5/2 - x_\beta + 2x_\nu\right)$ (gyro-Bohm transport assumed). For $x_\nu = -1/2$, the density exponent $\alpha_n = 0$ independently of $\beta$ scaling. For $x_\nu < -1/2$ the density exponent becomes negative. To summarise, the collisionality dependence inferred from MAST global energy confinement data can be bracketed with $x_\nu = \text{from} -3/4 \text{ to} -1/2$. Note that dedicated collisionality scans in conventional tokamaks find the values of $x_\nu$ in the range from -0.25 to -0.75 [13]. Therefore the plasmas in the present MAST dataset can be ranked among those with stronger collisionality dependence of energy confinement.

While the sum of the $I_P$ and $B_T$ exponents is controlled mainly by collisionality scaling the partition between them is mainly given by the safety factor exponent: $\alpha_I/(\alpha_B+\alpha_I) = -x_q/(2-2x_\beta)$. For MAST, the findings of sections 3, 4 and 5 can be summarised as: $\alpha_I/(\alpha_B+\alpha_I) = 0.24 \div 0.32$. These values can be matched by inverse-linear $q$ dependence, $x_q = -1$, if one assumes that confinement degrades with $\beta$ as $x_\beta =$ from -1 to -0.6. The $q$ dependence could be even weaker with $x_q = -0.65$, if confinement is $\beta$ independent. Such $q$ dependence is clearly weaker than in conventional tokamaks. In IPB98(y,2) scaling, the plasma current scaling dominates over the toroidal field with the value of $\alpha_I/(\alpha_B+\alpha_I)$ about 3 times larger than on MAST and consequently $x_q = -3$ [1]. In dedicated experiments in conventional tokamaks the $q$ dependence is found somewhat weaker with $x_q = -2.4$ [14].

This interpretation based on global parameters is supported by analysis of local heat transport of the two point scans already presented in section 5. For the $I_P$ scan, the analysis is shown in figure 4d. As mentioned above, the ion temperature $T_i$ is measured with a neutral particle analyser and shows that $T_e \approx T_i$ at mid radius (figure 4c). Assuming $T_e \approx T_i$ for all relevant radii we can calculate the effective heat diffusivity as $\chi_{eff} = -q_T/2n_e\nabla T_e$. The ratio of heat diffusivities in the outer half of the plasma is found to be $\chi_{eff}(1MA)/\chi_{eff}(0.6MA) \approx 0.8-1$ (see figure 4d). Such a value is almost 2 times lower than predicted by simple gyro-Bohm transport $\chi_{eff} \propto \chi_{gB}$. This discrepancy can be reconciled by invoking a linear dependence of effective heat diffusivity on safety factor $q$, $\chi_{eff} \propto \chi_{gB} q$. Note that this is weaker than in conventional aspect tokamaks where $\chi_{eff} \propto \chi_{gB} q^{-x_q}$ with $x_q \sim$ from $-1.5$ to $-2$ is measured [15]. This is in line with observations for the global energy confinement time discussed in above. Figure 4d also shows that within the error bars the measured ratio of diffusivities would be consistent with collisionality dependence $\chi_{eff} \propto \chi_{gB} q \nu_*^{-x\nu}$ with $x_\nu \sim -1/2$ (here $\nu_* \propto n_e/T_e^2$ i. e. without the $q$ dependence). The scaling with $\nu_*$ could be even stronger if one assumes a dependence on toroidal $\beta$ of the form of $\chi_{eff} \propto \chi_{gB} q \beta \nu_*^{-x_\nu}$ (see figure 4d).

Similar heat transport analysis for the two point $B_T$ scan is shown in figure 5d. The ratio of effective heat flux diffusivities between two plasmas, $\chi_{eff}(0.45T)/\chi_{eff}(0.34T)$, is 2 times lower than expected by a model $\chi_{eff} \propto \chi_{gB} q$ alone. Agreement can be obtained by adding a collisionality dependence of the form of $\chi_{eff} \propto \chi_{gB} q \nu_*^{-x_\nu}$ with $x_\nu = -2/3$ or perhaps even stronger. Invoking a dependence on toroidal $\beta$ of the form of $\chi_{eff} \propto \chi_{gB} q \beta \nu_*^{-x_\nu}$ has the same effect as a further increase of collisionality dependence (see figure 5d).

**7. Discussion and conclusion**

Analysis of MAST experimental data have shown that the energy confinement time displays a stronger-than-linear dependence on toroidal magnetic field. This confirms the observation on the NSTX spherical tokamak [7]. These results are in contrast to conventional IPB98(y,2) scaling which has been used so far for prediction towards fusion reactors based on spherical tokamaks. As mentioned in the introduction an example of such a device is the Component Test Facility (ST-CTF). This device is a volume neutron source aimed for testing components in neutron fluxes expected in power plants. ST-CTF is designed to generate 35MW of fusion power with a MAST-size plasma [4]. According to the IPB98(y,2) scaling such fusion power is produced if the normalised thermal energy confinement time is $H \equiv \tau_{E,th}/\tau_{IPB98y2} = 1.3$ and engineering parameters are set to $I_p = 6.5MA$, $B_T \sim 2.47T$, $\bar{n}_e = 1.1\times10^{20} m^{-3}$, $\kappa = 2.4$, $P_{aux} = 44MW$. It is now useful to see how these predictions change if one uses scalings based solely on data from spherical tokamaks. Energy confinement scaling derived from MAST data is given by equation (1). This scaling with correction for fast ion content estimated in section 4, $\tau_{E,th} = 0.74\times W_{mag}/P_L$, then gives the thermal energy confinement time as:

$$\tau_{E,th} = 0.186\, I_p^{0.59} B_T^{1.4} P_L^{-0.73} \qquad (6)$$

where the units are s, MA, T and MW respectively. This scaling predicts that for the ST-CTF device, with engineering parameters given above, the thermal energy confinement time normalised to IPB98(y,2) scaling is $H \sim 1.6$. Here, elongation, $\kappa$, and effective mass, $M$, exponents are taken from IPB98(y,2) scaling, though NSTX indicates a weaker $\kappa$ dependence [8]. A similar result is obtained using the scaling derived from NSTX data. Scaling 3 in table 1 in [8], with IPB98(y,2)-like $\kappa$ and $M$ exponents, gives for ST-CTF the normalised energy confinement time of $H \sim 1.8$. These favourable predictions towards ST-CTF are the result of the strong $B_T$ dependence in both the MAST and NSTX scalings. If such strong $B_T$

dependence is proved to be universal, it could allow re-optimisation of the ST-CTF engineering parameters in order to ease the requirements on its most critical parts such as the divertor and neutral beams.

The question of universality of strong $B_T$ scaling in spherical tokamaks, however, deserves careful attention. If such dependence is indeed the result of strong $\nu_*$ scaling, as suggested in this work, then one might expect that this dependence will become weaker towards lower $\nu_*$ values. This follows from the observation in conventional tokamaks where the $\nu_*$ dependence becomes weaker as plasmas become less collisional [13]. The importance of understanding the collisionality scaling is also stressed by the fact that $\nu_*$ is the main dimensionless plasma physics variable along which the confinement is extrapolated from MAST to ST-CTF [5]. It can be noted that the plasmas with highest $I_p$ and lowest $B_T$ from two point scans in section 5 form a collisionality scan with span of a factor of 2. A quick estimate of $\nu_*$ scaling is in line with the results found in section 6. This scan, however, is not perfect and the values of $\rho_*$, $\beta$ and $q$ differ by up to $\pm 12\%$ between these two plasmas. To improve this match and to increase the range of $\nu_*$ dedicated experiments are required.

**Acknowledgement**

This work was funded jointly by the United Kingdom Engineering and Physical Sciences Research Council and by the European Communities under the contract of Association between EURATOM and UKAEA. The views and opinions expressed herein do not necessarily reflect those of the European Commission.

**References**

[1] ITER Physics Basis, 1999 *Nucl. Fusion* **39** 2204
[2] ITER Final Design Report 2001, http://www.iter.org/a/index_nav4.htm
[3] Maisonnier D. *et al* 2007 *Nucl. Fusion* **47** (2007) 1524
[4] Voss G. *et al* 2007 *Fusion Eng. Design* doi:10.1016/j.fusengdes.2008.05.002
[5] Valovič M. *et al* 2005 *Nucl. Fusion* **45** 942
[6] Kaye S. *et al* 2006 *Plasma Phys. Control. Fusion* **48** A429
[7] Kaye S. *et al* 2007 *Nucl. Fusion* **47** 499
[8] Kaye S. *et al* 2006 *Nucl. Fusion* **46** 848
[9] TRANSP code http://w3.pppl.gov/transp/
[10] Fuller W. A. 1987 Measurement Error Models (New York: Wiley) chapter 4
[11] Cordey J. G. *et al* 2005 *Nucl. Fusion* **45** 1078
[12] McDonald D. C. *et al* 2007 *Nucl. Fusion* **47** 147
[13] Luce T. C., Petty C. C. and Cordey J. G. 2008 *Plasma Phys. Control. Fusion* **50** 043001
[14] Petty C C *et al* 1998 *Phys. Plasmas* **5** 1695
[15] Garbet, X. *et al* 2004 *Plasma Phys. Control. Fusion* **46** 1351